J BONE ONCOL 48 (2024) 100640

Contents lists available at ScienceDirect

Journal of Bone Oncology

journal homepage: www.elsevier.com/locate/jbo

AI diagnostics in bone oncology for predicting bone metastasis in lung cancer patients using DenseNet-264 deep learning model and radiomics

Taisheng Zeng [a,b,c,*], Yusi Chen [a,b,c], Daxin Zhu [a,b,c], Yifeng Huang [d], Ying Huang [d], Yijie Chen [e], Jianshe Shi [e], Bijiao Ding [d], Jianlong Huang [a,b,c,**]

[a] Faculty of Mathematics and Computer Science, Quanzhou Normal University, Quanzhou 362000, China
[b] Fujian Provincial Key Laboratory of Data Intensive Computing, Quanzhou 362000, China
[c] Key Laboratory of Intelligent Computing and Information Processing, Fujian Province University, Quanzhou 362000, China
[d] Department of Diagnostic Radiology, Huaqiao University Affliated Strait Hospital, Quanzhou, Fujian 362000, China
[e] Department of General Surgery, Huaqiao University Affliated Strait Hospital, Quanzhou, Fujian 362000, China

HIGHLIGHTS

- DenseNet-264 predicts bone metastasis in lung cancer patients.
- DenseNet-264 outperforms traditional radiomics models with better AUC on training and validation sets.
- Predictive model facilitates early intervention and personalized treatment.
- Clinical utility of deep learning for detecting bone metastasis in lung cancer patients.

ARTICLE INFO

Keywords:
Bone Metastasis
DenseNet-264
Deep Learning Diagnosis
Radiomics
Cancer

ABSTRACT

This study aims to predict bone metastasis in lung cancer patients using radiomics and deep learning. Early prediction of bone metastasis is crucial for timely intervention and personalized treatment plans. This can improve patient outcomes and quality of life. By integrating advanced imaging techniques with artificial intelligence, this study seeks to enhance predictive accuracy and clinical decision-making.

Methods: We included 189 lung cancer patients, comprising 89 with non-bone metastasis and 100 with confirmed bone metastasis. Radiomic features were extracted from CT images, and feature selection was performed using Minimum Redundancy Maximum Relevance (mRMR) and Least Absolute Shrinkage and Selection Operator (LASSO). We developed and validated a radiomics model and a deep learning model using DenseNet-264. Model performance was evaluated using the area under the receiver operating characteristic curve (AUC), accuracy, sensitivity, and specificity. Statistical comparisons were made using the DeLong test.

Results: The radiomics model achieved an AUC of 0.815 on the training set and 0.778 on the validation set. The DenseNet-264 model demonstrated superior performance with an AUC of 0.990 on the training set and 0.971 on the validation set. The DeLong test confirmed that the AUC of the DenseNet-264 model was significantly higher than that of the radiomics model ($p < 0.05$).

Conclusions: The DenseNet-264 model significantly outperforms the radiomics model in predicting bone metastasis in lung cancer patients. The early and accurate prediction provided by the deep learning model can facilitate timely interventions and personalized treatment planning, potentially improving patient outcomes. Future studies should focus on validating these findings in larger, multi-center cohorts and integrating clinical data to further enhance predictive accuracy.

* Corresponding author at: Faculty of Mathematics and Computer Science, Quanzhou Normal University, Quanzhou 362000, China.
** Corresponding author at: Faculty of Mathematics and Computer Science, Quanzhou Normal University, Quanzhou 362000, China.
E-mail addresses: ztsjacky@qztc.edu.cn (T. Zeng), robotics@qztc.edu.cn (J. Huang).

https://doi.org/10.1016/j.jbo.2024.100640
Received 23 June 2024; Received in revised form 14 September 2024; Accepted 21 September 2024
Available online 26 September 2024

1. Introduction

Lung cancer is one of the most common and deadly cancers globally. It accounts for a large number of cancer-related deaths and illnesses [1,2]. Despite advances in diagnostic and therapeutic strategies, the prognosis for lung cancer patients remains poor, primarily due to its propensity for early dissemination and metastasis [3]. Bone metastasis is a common complication, affecting 30–40 % of lung cancer patients. This severely impacts clinical management, quality of life, and survival outcomes [4]. This phenomenon not only complicates the clinical management of lung cancer but also significantly impacts the quality of life and survival outcomes for affected individuals [5–8]. Bone metastasis is a common and severe complication in lung cancer patients, significantly affecting prognosis and quality of life. Early detection of bone metastasis is crucial for timely intervention and effective management. However, predicting bone metastasis using conventional clinical and imaging methods remains challenging.

Bone metastasis in lung cancer patients is associated with a spectrum of debilitating symptoms, including severe pain, pathological fractures, hypercalcemia, and spinal cord compression, all of which contribute to increased morbidity and healthcare burden [9]. The clinical management of bone metastasis typically involves a combination of systemic therapies, such as chemotherapy, targeted therapy, and immunotherapy, alongside local treatments like radiotherapy and surgery [10,11]. Despite these multimodal treatment approaches, the prognosis for patients with bone metastasis remains dismal, with median survival rates often not exceeding 12 months following diagnosis of metastatic spread [12].

The early prediction of bone metastasis in lung cancer patients holds paramount importance for several reasons [13]. First and foremost, bone metastasis is often associated with severe complications such as debilitating pain, pathological fractures, hypercalcemia, and spinal cord compression, which significantly impair the quality of life of affected individuals and can lead to substantial morbidity and mortality [14]. Early detection allows for timely intervention, potentially mitigating these complications and improving overall patient outcomes. From a healthcare management perspective, early prediction of bone metastasis can optimize resource allocation, ensuring that patients receive the appropriate level of care at the right time. This can lead to more efficient use of healthcare resources, reducing unnecessary hospitalizations and procedures, and ultimately lowering the overall cost of care for lung cancer patients [15].

Given the clinical importance of bone metastasis in lung cancer and the significant challenges associated with its management, there is an urgent need for effective strategies to predict its occurrence [4,16,17]. Early prediction and intervention can potentially mitigate the complications associated with bone metastasis, improve patient outcomes, and optimize resource allocation within healthcare systems [18,19]. However, current predictive models are limited by their reliance on traditional imaging techniques and clinical parameters, which often fail to capture the complex biological underpinnings of metastatic spread. This underscores the necessity for innovative approaches that integrate advanced technologies to enhance predictive accuracy and clinical utility [20].

Radiomics and deep learning represent two cutting-edge approaches in the field of medical imaging analysis, offering significant potential for predicting bone metastasis in lung cancer patients. Radiomics involves the extraction of a large number of quantitative features from medical images, which capture the underlying tumor phenotype and microenvironment in a non-invasive manner [21]. These features, which include texture, shape, and intensity, can be used to develop predictive models that provide insights into tumor behavior and progression [22]. By converting medical images into high-dimensional data, radiomics allows for a comprehensive analysis that goes beyond traditional visual assessment, enhancing the ability to detect subtle patterns associated with metastatic potential.

Deep learning, particularly convolutional neural networks (CNNs), has revolutionized the field of medical imaging by enabling the automated extraction and analysis of complex patterns from large datasets [23]. CNNs are designed to automatically learn hierarchical features from input images through multiple layers of convolutional operations, making them highly effective for tasks such as image classification, segmentation, and detection. In the context of predicting bone metastasis, deep learning models can analyze lung cancer CT scans to identify features indicative of metastatic spread, often achieving higher accuracy and robustness compared to traditional methods [24].

The integration of radiomics and deep learning has led to a new paradigm in predictive modeling. Studies have demonstrated that combining radiomic features with deep learning algorithms can significantly improve the predictive performance for various clinical outcomes, including metastasis and survival. For instance, research has shown that radiomics-based models can successfully predict bone metastasis in lung cancer patients by analyzing CT images to identify textural and morphological changes associated with metastatic disease. Furthermore, deep learning models, trained on large datasets of annotated images, have been able to achieve high accuracy in distinguishing between metastatic and non-metastatic cases, offering a powerful tool for early detection and risk stratification.

Recent advancements in this field have also explored the use of multimodal approaches, where radiomics features are combined with clinical data, genomic information, and other imaging modalities such as PET and MRI, to further enhance predictive accuracy. This holistic approach allows for a more comprehensive understanding of the tumor and its metastatic potential, leading to more personalized and effective treatment strategies.

The application of radiomics and deep learning in predicting bone metastasis represents a significant advancement in the field of oncology. These technologies offer a promising avenue for early detection and personalized treatment planning, ultimately improving patient outcomes and quality of life. This study aims to utilize radiomics and deep learning to predict the risk of bone metastasis based on CT scans of lung cancer, highlighting its important clinical significance. Incorporating the predictive capabilities of the deep learning model into clinical workflows has the potential to significantly enhance the management of lung cancer patients at risk of bone metastasis. Early identification of high-risk patients can facilitate timely interventions, potentially improving prognosis and quality of life. Additionally, the model can aid in personalizing treatment plans by providing insights into individual risk profiles, thereby optimizing therapeutic strategies. Efficient risk stratification also allows for better allocation of healthcare resources, ensuring that patients who are most likely to benefit from intensive monitoring and treatment receive the necessary attention.

2. Methodology

2.1. Data collection

In this study, patients were selected based on specific inclusion and exclusion criteria to ensure a representative study population. The inclusion criteria were: (1) a confirmed diagnosis of primary lung cancer, (2) availability of CT imaging data at initial diagnosis and during follow-up, (3) histopathological confirmation of bone metastasis or no bone metastasis within ten years post-diagnosis, and (4) provision of informed consent. The exclusion criteria were: (1) incomplete medical records or missing CT imaging data, (2) a history of other malignancies, (3) prior treatments interfering with bone metastasis assessment, and (4) insufficient follow-up data. These criteria were established to ensure the robustness and generalizability of our findings. We aim to collect a comprehensive dataset comprising a total of 189 samples to facilitate the development and validation of our predictive models for bone metastasis in lung cancer patients. The dataset will include:

- 89 patients with primary lung cancer and non-bone metastasis
- 100 patients with bone metastasis: These cases will include patients who have developed bone metastasis from primary lung cancer. This group is crucial for training the model to recognize patterns and features indicative of metastatic spread to the bones. An example of enrolled patients with bone metastasis is shown in Fig. 1.

Inclusion Criteria:

- Patients with a confirmed diagnosis of primary lung cancer.
- Patients with CT imaging data available at the time of initial diagnosis and during follow-up periods.
- Patients with histopathological confirmation of bone metastasis or confirmation of no bone metastasis within ten years following the initial lung cancer diagnosis.
- Patients who provided informed consent for the use of their medical data for research purposes.

Exclusion Criteria:

- Patients with incomplete medical records or missing CT imaging data.
- Patients wipatients with primary lung cancer th a history of other malignancies that could affect bone metastasis.
- Patients who received treatments that could interfere with the assessment of bone metastasis, such as bisphosphonates, prior to the initial lung cancer diagnosis.
- Patients with insufficient follow-up data to confirm the presence or absence of bone metastasis.

By including these detailed criteria, we aim to ensure that the study population is representative and that the findings are robust and generalizable. This approach helps to minimize selection bias and ensures that the study outcomes are reliable.

Data Sources

- Hospital Databases: Data will be collected from electronic medical records and imaging archives of collaborating hospitals.
- Imaging Data: All CT scans will be retrieved from the hospital's radiology department, ensuring that the imaging protocols are consistent and standardized across all samples.

Data Preprocessing

- Image Normalization: All CT images will be preprocessed to standardize the pixel intensity values to a common scale, facilitating consistent feature extraction.
- Segmentation: Regions of interest (ROIs) corresponding to lung cancer primary lesions in chest CT scans will be manually segmented by experienced radiologists using software such as ITK-SNAP as show in Fig. 2.
- Quality Control: Each segmented image will undergo a quality check to ensure accuracy and consistency in segmentation. Any discrepancies will be reviewed and corrected by a consensus of radiologists.

Ethical Considerations

- Ethical Approval: The study protocol will be reviewed and approved by the Institutional Review Board (IRB) of the participating hospitals.
- Informed Consent: Informed consent will be obtained from all patients or their legal representatives prior to inclusion in the study.

Data Splitting

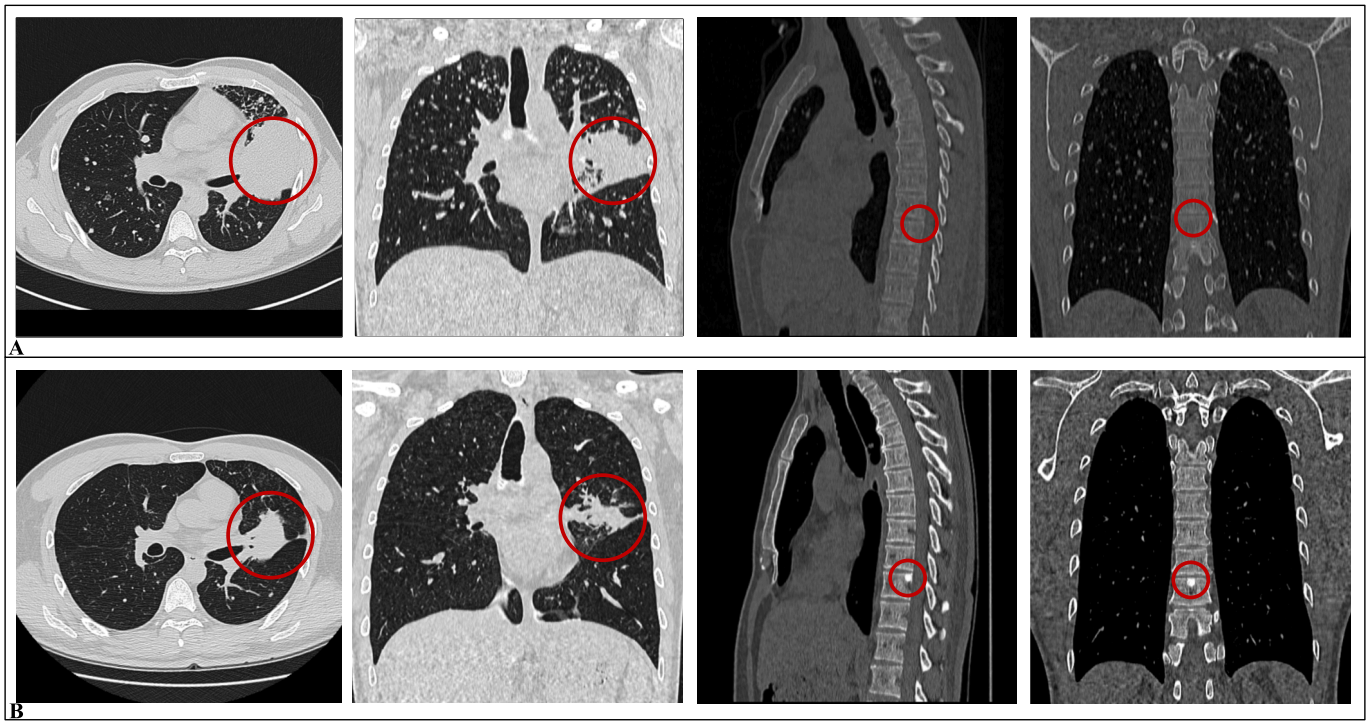

Fig. 1. CT Images of a Patient with Bone Metastasis. (A) Initial diagnosis of lung cancer. The first row shows CT images of a patient at the time of initial lung cancer diagnosis. The leftmost image depicts the lung tumor, while the subsequent images display the thoracic spine (T10) without any signs of bone metastasis (as indicated by the absence of abnormalities in the red circled area). (B) Follow-up CT images six months later. The second row shows the CT images of the same patient six months after the initial diagnosis. The leftmost image indicates an improvement in the lung tumor following treatment. However, the subsequent images show the development of bone metastasis in the thoracic spine (T10), marked by red circles highlighting the metastatic lesions. (For interpretation of the references to colour in this figure legend, the reader is referred to the web version of this article.)

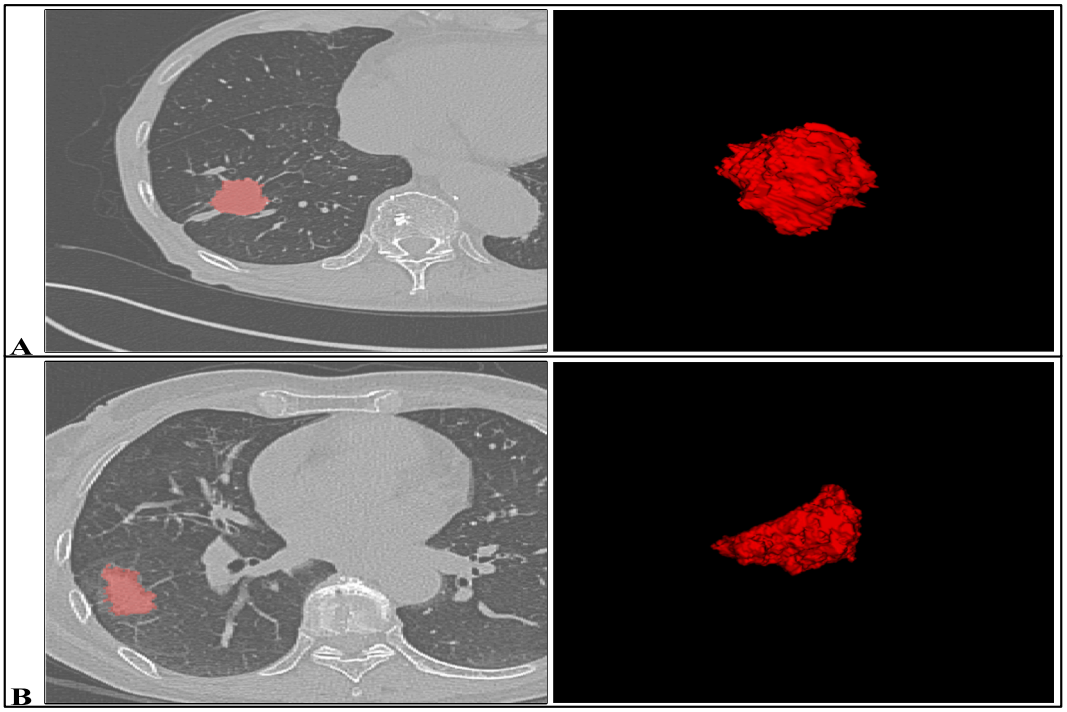

Fig. 2. Segmentation of lung cancer primary lesions in chest CT scans. (A) Example of a primary lung lesion in a patient without bone metastasis. The left panel shows the CT scan with the segmented lesion highlighted in red, while the right panel displays the 3D reconstruction of the segmented lesion. (B) Example of a primary lung lesion in a patient with bone metastasis. The left panel shows the CT scan with the segmented lesion highlighted in red, while the right panel displays the 3D reconstruction of the segmented lesion. The regions of interest (ROIs) were manually segmented by experienced radiologists using software such as ITK-SNAP. (For interpretation of the references to colour in this figure legend, the reader is referred to the web version of this article.)

The dataset will be divided into two parts: 70 % of the samples will be used as the training set, and the remaining 30 % will be used as the validation set. This split ensures that the model is trained on a sufficient amount of data while also being rigorously tested on an independent validation set to assess its performance and generalizability. Table 1 summarizing the dataset split:

This dataset will serve as the foundation for training and validating our radiomics and deep learning models, providing a robust basis for predicting the risk of bone metastasis in lung cancer patients.

As illustrated in Fig. 3, the workflow of this study involves several key steps. After independently splitting the dataset into training and validation sets, we apply radiomics and deep learning techniques to develop and validate predictive models for bone metastasis in lung cancer patients. For the radiomics approach, we first extract radiomic features from the CT images. Following feature extraction, we employ Minimum Redundancy Maximum Relevance (mRMR) and Least Absolute Shrinkage and Selection Operator (LASSO) methods for feature selection. These selected features are then used to build the predictive model. The performance of this model is validated using the validation set. For the deep learning approach, we utilize the DenseNet-264 architecture to build the predictive model. The validation set is then used to assess the performance of this deep learning model. Finally, we compare the performance of the two models using statistical tests such as the DeLong test to evaluate their predictive accuracy and robustness.

Table 1
Dataset split for training and validation.

Dataset split	Positive cases (Bone Metastasis)	Negative cases (None-Bone Metastasis)	Total samples	Percentage of total
Training	70	62	132	70
Validation	30	27	57	30
Total	100	89	189	100

This comparative analysis helps in determining the most effective approach for predicting bone metastasis in lung cancer patients [19].

2.2. Feature extraction and selection

Radiomic features were extracted from the CT images using the open-source software Pyradiomics. A total of 1316 features, including shape, texture, and intensity, were extracted from the segmented lung tumors. To reduce dimensionality and select the most relevant features, we employed Minimum Redundancy Maximum Relevance (mRMR) followed by Least Absolute Shrinkage and Selection Operator (LASSO) regression. The mRMR method selected 30 features, which were further refined to 8 features using LASSO.

- Extracting imaging features using radiomics techniques

Radiomics involves the extraction of a large number of quantitative features from medical images, capturing the underlying tumor phenotype and microenvironment. These features include shape, texture, intensity, and wavelet features, which provide a comprehensive description of the tumor's characteristics. The extracted features can highlight subtle differences that are not discernible through visual inspection alone. From the chest CT scans of lung tumors, we extracted a total of 1,316 radiomic features. These features provide a detailed and quantitative assessment of the tumor, which is essential for building accurate predictive models [25].

- Feature Selection using mRMR and LASSO

To enhance the predictive power of the radiomic features, we apply feature selection methods, namely Minimum Redundancy Maximum Relevance (mRMR) and Least Absolute Shrinkage and Selection Operator (LASSO)[26]:

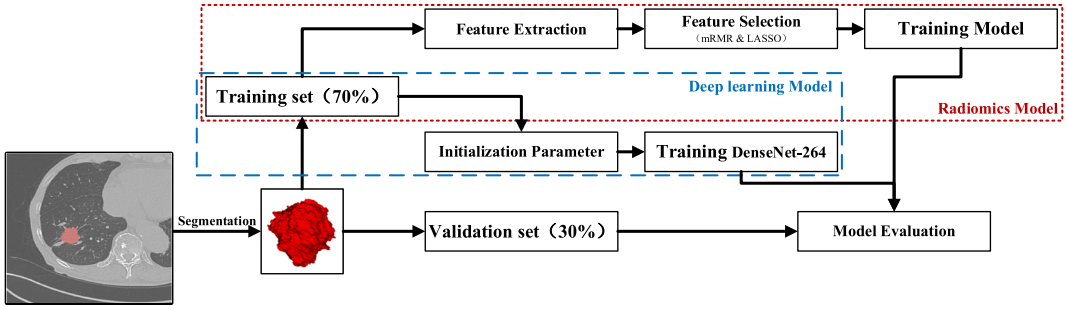

Fig. 3. Workflow of the study on predicting bone metastasis in lung cancer patients using radiomics and deep learning techniques.

- Minimum Redundancy Maximum Relevance (mRMR)

mRMR was used to select features that are highly relevant to the target variable (bone metastasis) while ensuring minimal redundancy among the features. This method ranks features based on their mutual information with the target variable and their correlation with other features, selecting those that provide the most unique information.

- Least Absolute Shrinkage and Selection Operator (LASSO)

LASSO regression was applied to further refine the feature set selected by mRMR. LASSO adds an L1 regularization term to the logistic regression model, which shrinks less important feature coefficients to zero, effectively performing feature selection. The features with non-zero coefficients after LASSO regression were considered important for the model's predictions. These selected features are then used to build a predictive model, which is subsequently validated using the validation dataset. This process ensures that the model is both accurate and generalizable to new, unseen data [27].

2.3. Model development

The model development process in this study involves the application of a 3D deep learning model, specifically using the DenseNet-264 architecture. This approach is designed to leverage the spatial and contextual information present in the 3D CT images to improve the accuracy of bone metastasis prediction.

Selection of Deep Learning Models

For the deep learning component of this study, we selected the DenseNet-264 architecture, which is well-regarded for its efficiency in learning complex features from medical images. DenseNet (Dense Convolutional Network) is known for its ability to facilitate feature reuse through dense connections, which connect each layer to every other layer in a feed-forward manner. This architecture helps in alleviating the vanishing gradient problem, improving feature propagation, and reducing the number of parameters, making it an ideal choice for our predictive modeling task.

The key components of the DenseNet-264 model architecture include

The DenseNet-264 model is a sophisticated deep learning architecture designed to efficiently process and analyze volumetric CT data for predicting bone metastasis in lung cancer patients. Here is a detailed description of its structure, including the specific layers in each dense block:

- Input CT Volume: The input to the model is the volumetric CT scan of the patient's lungs. This input is a 3D array of voxel intensities representing the anatomical structures within the scanned volume.
- Dense Block 1 (H1)

Layers: 12 convolutional layers

Description: The first dense block consists of 12 convolutional layers. Each layer receives input from all preceding layers within the same block, enhancing feature reuse and improving gradient flow. This block captures initial features from the input CT volume, including edges and simple textures.

- Transition Layer 1

Function: Down-sampling

Description: This layer reduces the spatial dimensions of the feature maps using a combination of batch normalization, a 1x1 convolutional layer, and an average pooling layer. This down-sampling helps to reduce computational complexity while retaining important features.

- Dense Block 2 (H2)

Layers: 24 convolutional layers

Description: The second dense block includes 24 convolutional layers. Similar to Dense Block 1, each layer in this block receives inputs from all preceding layers within the block. This extensive connectivity allows the network to learn more complex features and patterns from the input data.

- Transition Layer 2

Function: Down-sampling

Description: Another transition layer, similar in structure and function to Transition Layer 1, further reduces the spatial dimensions of the feature maps.

- Dense Block 3 (H3)

Layers: 128 convolutional layers

Description: The third dense block is significantly deeper, with 128 convolutional layers. This block is crucial for learning highly complex and abstract features from the CT data. The dense connectivity ensures that features learned at earlier layers are available to all subsequent layers, enhancing the model's ability to capture intricate details.

- Transition Layer 3

Function: Down-sampling

Description: This transition layer continues the process of reducing the spatial dimensions of the feature maps, ensuring that the input to the next dense block is of manageable size.

- Dense Block 4 (H4)

Layers: 96 convolutional layers

Description: The fourth dense block consists of 96 convolutional layers. This block further refines the features extracted by the previous layers, focusing on the most relevant patterns for predicting bone metastasis.

- Global Average Pooling

Function: Feature map reduction

Description: Before the final classification layer, global average pooling is applied to reduce each feature map to a single value by averaging all the values in the feature map. This reduces the spatial dimensions to a single vector for each feature map, making the data ready for classification while minimizing overfitting.

- Fully Connected Layer (Softmax)

Function: Classification

Description: The final layer is a fully connected layer that outputs the probability of bone metastasis presence. It uses a softmax activation function to provide a normalized probability distribution over the possible classes (presence or absence of bone metastasis).3D Convolutions: Adapted from the standard 2D convolutions, 3D convolutions process the volumetric CT data, allowing the model to learn spatial features across the entire volume.

- Batch Normalization and ReLU Activations: Used after each convolutional layer to stabilize and accelerate the training process.
- Global Average Pooling: Applied before the final classification layer to reduce the spatial dimensions of the feature maps to a single vector for each feature map.
- Fully Connected Layer: The final layer that outputs the probability of bone metastasis presence, using a softmax activation function for classification.

The specific structure of the DenseNet-264 model is illustrated in Fig. 4.

Model Training and Optimization

The DenseNet-264 model is trained using the training set (70 % of the dataset) and validated on the validation set (30 % of the dataset). Key steps in the training process include:

Data Preprocessing: Resize images to uniform dimensions, normalize pixel intensities, and augment the data to enhance model generalization. We employed the DenseNet-264 architecture, configured as a 3D convolutional neural network. For the DenseNet-264 deep learning model, several hyperparameters were tuned to optimize performance. These included:

- Learning Rate: A range of learning rates (e.g., 0.0001, 0.001, 0.01) was tested using a grid search approach. The learning rate of 0.001 was selected based on its ability to provide stable convergence and minimize validation loss.
- Batch Size: Different batch sizes (e.g., 8, 16, 32) were evaluated. A batch size of 64 was chosen to balance computational efficiency and model performance.
- Number of Epochs: The model was initially trained for up to 2000 epochs. An early stopping mechanism with a patience of 10 epochs was implemented to prevent overfitting. The final number of epochs was determined based on the point at which the validation loss plateaued.

The hyperparameter tuning process involved multiple iterations of training and validation to identify the optimal combination of hyperparameters. Grid search with cross-validation was used to systematically evaluate each combination, ensuring that the chosen hyperparameters provided the best performance on the validation set. Data augmentation techniques, such as rotation and flipping, were applied to enhance model robustness.

Hyperparameter Tuning: Optimize learning rate, batch size, and number of epochs to achieve the best performance.

Loss Function: Use cross-entropy loss for classification tasks, minimized using backpropagation and gradient descent.

Both models were validated using the independent validation set. Cross-validation with 10-folds was performed to ensure robustness. Statistical comparison of model performance was conducted using the DeLong test.

2.4. Model evaluation

The evaluation of the developed predictive models involves several key metrics and methodologies to ensure their accuracy, reliability, and generalizability.

To comprehensively assess the performance of the predictive models, the following evaluation metrics will be used:

Accuracy: The proportion of true positive and true negative predictions among the total number of cases.

Sensitivity (Recall): The ability of the model to correctly identify patients with bone metastasis (true positive rate).

Specificity: The ability of the model to correctly identify patients without bone metastasis (true negative rate).

Area Under the ROC Curve (AUC): A measure of the model's ability to distinguish between patients with and without bone metastasis, with higher values indicating better discriminative performance.

Cross-Validation Methods

The radiomics model was validated using an independent validation set, which comprised 30 % of the total dataset. In addition to this, a 10-fold cross-validation technique was employed to assess the model's robustness. In 10-fold cross-validation, the dataset is randomly partitioned into ten equal-sized folds. Each fold is used once as the validation set, while the remaining nine folds form the training set. This process is repeated ten times, and the results are averaged to provide a comprehensive evaluation of the model's performance. The performance metrics assessed included AUC, accuracy, specificity, and sensitivity.

Similarly, the DenseNet-264 deep learning model was validated using the same independent validation set and 10-fold cross-validation technique. During each fold, the model was trained on 90 % of the data and validated on the remaining 10 %. This process ensured that the model's performance metrics were robust and not dependent on a specific subset of the data. The early stopping mechanism with a patience of 10 epochs was also employed to prevent overfitting during training. To compare the performance of different predictive models, the DeLong test will be utilized.

To evaluate and compare the performance of the radiomics and deep learning models, we employed several statistical tests, including the DeLong test, to assess the differences in the area under the receiver operating characteristic curves (AUCs).

The DeLong test is a non-parametric method used to compare the AUCs of two correlated receiver operating characteristic (ROC) curves.

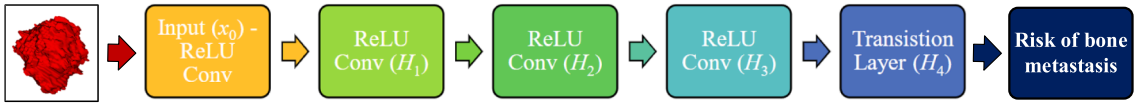

Fig. 4. The specific structure of the DenseNet-264 model. The architecture includes the following key components: Input layer (X_0) followed by a ReLU convolutional layer. A series of ReLU convolutional layers (H_1, H_2, H_3) to process the input features. Transition layer (H_4) to reduce the spatial dimensions and number of feature maps. The final output layer that predicts the risk of bone metastasis.

This test is particularly suitable for comparing the performance of two diagnostic tests or predictive models when applied to the same set of patients. The DeLong test evaluates whether the difference between the AUCs of two models is statistically significant by generating a p-value. A low p-value (typically < 0.05) indicates that the difference in AUCs is statistically significant.

To evaluate the clinical utility of the predictive models, we performed Decision Curve Analysis (DCA). DCA assesses the net benefit of different prediction models across various threshold probabilities. The analysis was conducted by plotting the net benefit curves for the DenseNet-264 model. Threshold probabilities ranging from 0.05 to 0.95 were selected to cover a wide range of clinical decision thresholds[28].

By employing these evaluation metrics and methodologies, we aim to rigorously validate the predictive models and ensure their clinical applicability in predicting bone metastasis in lung cancer patients.

3. Experimental results

3.1. Dataset description

- Basic statistics of the dataset

The basic statistics of the dataset, as summarized in Table 2, show that there are no significant differences between the training and validation sets across various clinical variables, including age, gender distribution, height, weight, BMI, and smoking status. Similarly, when comparing patients with and without bone metastasis, the differences in these clinical variables are not statistically significant, with all p-values greater than 0.05 but less than 0.10. This indicates that the groups are well-matched and comparable, ensuring that any observed differences in model performance are likely due to the model itself rather than underlying differences in the dataset composition.

3.2. Results analysis

- Impact of radiomics features on prediction results

In this study, we evaluated the impact of radiomics features on the prediction of bone metastasis in lung cancer patients. The process involved two main steps: feature selection using Minimum Redundancy Maximum Relevance (mRMR) and Least Absolute Shrinkage and Selection Operator (LASSO).

Feature Selection Process

mRMR Feature Selection: Initially, we applied the mRMR method to select 30 features from the extracted radiomics features. This step ensured that the selected features had maximum relevance to the prediction target (bone metastasis) and minimal redundancy among themselves.

LASSO Feature Selection: Subsequently, we employed LASSO to further refine the selection, reducing the 30 features to the most predictive eight features. LASSO is a powerful regression analysis technique that performs both variable selection and regularization to enhance the prediction model's performance.

Visualization of Feature Selection

The results of the LASSO feature selection process are illustrated in Fig. 5. A panel of the figure shows the weight distribution of each selected feature, indicating their importance in the predictive model. B panel displays the LASSO path, illustrating the coefficient shrinkage process and the selection of the final eight features.

The features shown in Fig. 5 were selected through the feature selection process using Minimum Redundancy Maximum Relevance (mRMR) and Least Absolute Shrinkage and Selection Operator (LASSO). These features contribute significantly to the predictive performance of the radiomics model. Here is a detailed description of each feature:

(A) Feature Coefficients from LASSO Regression

- **wavelet_LHH_glcm_ZoneVariance**: This feature is derived from the Gray Level Co-occurrence Matrix (GLCM) after applying a wavelet transform (LHH). It measures the variance in the size of homogeneous zones within the tumor, indicating texture complexity.
- **lbp_3D_m2_firstorder_Skewness**: This feature comes from the Local Binary Patterns (LBP) 3D model, representing the skewness of the intensity distribution within the tumor, which highlights asymmetry in voxel intensity values.
- **gradient_glcm_GreyLevelNonUniformity**: Extracted from the GLCM based on the gradient image, this feature measures the variability in gray levels, reflecting texture homogeneity.
- **wavelet_HHH_firstorder_Median**: This feature is calculated from the first-order statistics of the wavelet-transformed (HHH) image. It represents the median intensity value within the tumor, providing insight into central tendency.
- **lbp_3D_ll_glcm_SumSquares**: Another LBP 3D feature, representing the sum of squared intensity values. It captures the spread of intensity values around the mean, indicating texture variability.
- **exponential_glszm_Busyness**: Derived from the Gray Level Size Zone Matrix (GLSZM), this feature measures the complexity and heterogeneity within the tumor based on zone busyness.
- **original_shape_Sphericity**: This shape feature quantifies how spherical the tumor is, providing geometric information about the tumor's form and compactness.
- **exponential_glcm_IdnEntropy**: This GLCM feature measures the entropy of the intensity distribution, indicating randomness and complexity in texture patterns.

(B) LASSO Path Plot

The LASSO path plot shows the regularization path for the selected features. The x-axis represents the regularization parameter (Lambda), and the y-axis shows the feature coefficients. The vertical dashed line indicates the optimal value of Lambda chosen during cross-validation, where the model achieves the best performance with the fewest number of features. Features with non-zero coefficients at this point are selected as the most predictive for the model.

Table 2
Basic statistics of the dataset.

Clinical information	Training set (n = 132)	Validation set (n = 57)	p-value	Bone metastasis (n = 100)	No bone metastasis (n = 89)	p-value
Age (years)	65.213 ± 10.134	66.047 ± 9.802	0.068	66.310 ± 9.654	64.578 ± 10.272	0.072
Gender						
– Male	75 (56.818 %)	32 (56.140 %)	0.082	58 (58.000 %)	49 (55.056 %)	0.065
– Female	57 (43.182 %)	25 (43.860 %)	0.082	42 (42.000 %)	40 (44.944 %)	0.065
Height (cm)	168.457 ± 9.389	169.004 ± 8.729	0.065	169.112 ± 8.654	168.101 ± 9.473	0.062
Weight (kg)	70.288 ± 12.212	71.096 ± 11.872	0.062	71.454 ± 11.946	69.112 ± 12.031	0.07
BMI (kg/m^2)	24.752 ± 3.102	24.944 ± 3.011	0.079	25.048 ± 3.056	24.612 ± 3.088	0.066
Smoking Status						
– Current Smoker	45 (34.091 %)	20 (35.088 %)	0.068	35 (35.000 %)	30 (33.708 %)	0.073
– Former Smoker	50 (37.879 %)	22 (38.596 %)	0.071	39 (39.000 %)	33 (37.079 %)	0.075
– Never Smoker	37 (28.030 %)	15 (26.316 %)	0.083	26 (26.000 %)	26 (29.213 %)	0.081

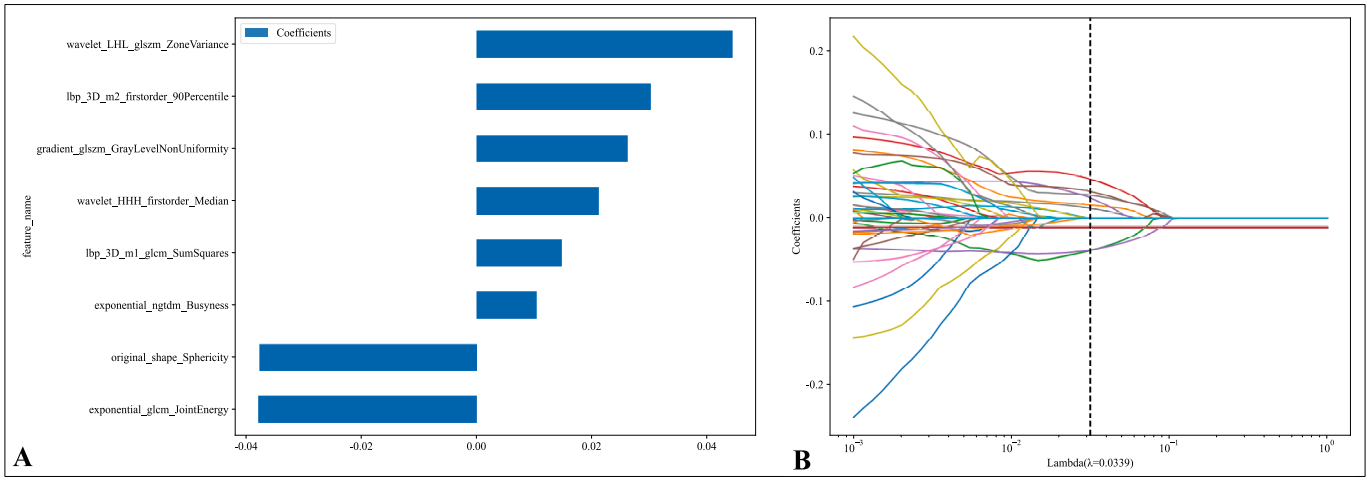

Fig. 5. Radiomics Feature Selection and Importance. (A) Weight distribution of the selected radiomics features after LASSO feature selection. The bar plot shows the coefficients of the eight most predictive features, indicating their relative importance in the predictive model.(B) LASSO coefficient path. This plot illustrates the process of LASSO feature selection, showing the coefficient trajectories of the radiomics features as a function of the regularization parameter (Lambda). The vertical dashed line indicates the optimal Lambda value where the final eight features are selected.

These selected features provide a comprehensive representation of the tumor's texture, shape, and intensity characteristics, contributing to the model's ability to predict bone metastasis in lung cancer patients accurately.

Performance of the radiomics models and deep learning models

The evaluation of various radiomics and deep learning models demonstrates significant differences in their predictive capabilities for bone metastasis in lung cancer patients. The performance metrics, including Area Under the Curve (AUC), Accuracy, Specificity, and Sensitivity, provide a comprehensive assessment of each model's effectiveness on both the training and test sets. Shown in Fig. 6 and Table 3, DenseNet-264 exhibits outstanding performance across all evaluation metrics, both in the training and test sets, highlighting its superior capability in predicting bone metastasis. In the training set, DenseNet-264 achieved an AUC of 0.990, an accuracy of 0.954, a specificity of 0.947, and a sensitivity of 0.981. In the test set, it maintained high performance with an AUC of 0.971, an accuracy of 0.966, a perfect specificity of 1.000, and a sensitivity of 0.833. These results indicate excellent discriminative ability and generalizability. DenseNet-121 also performed well, particularly in the training set, with an AUC of 0.995, an accuracy of 0.975, a specificity of 0.977, and a sensitivity of 0.965. However, its performance decreased in the test set, with an AUC of 0.939, an accuracy of 0.857, a specificity of 0.909, and a sensitivity of 0.667, indicating reduced generalizability compared to DenseNet-264. The Radiomics KNN model showed reasonable performance but was outperformed by both DenseNet models. It had an AUC of 0.905, an accuracy of 0.855, a specificity of 0.878, and a sensitivity of 0.767 in the training set, but its performance dropped significantly in the test set with an AUC of 0.732, an accuracy of 0.766, a specificity of 0.852, and a sensitivity of 0.433. The Radiomics Logistic Regression (LR) model showed moderate performance with an AUC of 0.815, an accuracy of 0.731, a specificity of 0.713, and a sensitivity of 0.800 in the training set.

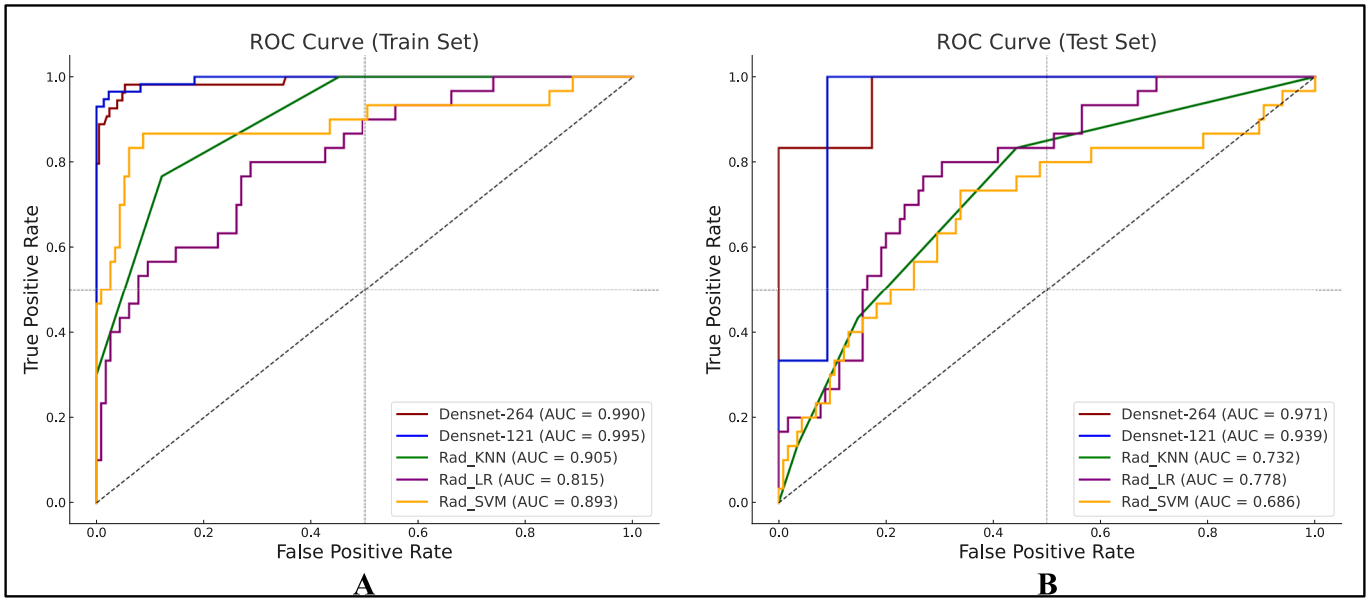

Fig. 6. Performance of Radiomics Models and Deep Learning Models. (A) ROC Curve for the training set. The curves depict the performance of different models, including DenseNet-264, DenseNet-121, Radiomics KNN, Radiomics Logistic Regression (LR), and Radiomics Support Vector Machine (SVM). The AUC values are listed in the legend, indicating the area under the ROC curve for each model. (B) ROC Curve for the test set. Similar to the training set, this plot shows the ROC curves for the same models, providing a comparative evaluation of their performance on unseen data.

Table 3
Performance metrics of radiomics and deep learning models.

Model	AUC	Accuracy	Specificity	Sensitivity	Group
Densnet-264	0.995	0.954	0.947	0.981	train
	0.971	0.966	1	0.833	test
Densnet-121	0.995	0.975	0.977	0.965	train
	0.939	0.857	0.909	0.667	test
Rad_KNN	0.905	0.855	0.878	0.767	train
	0.732	0.766	0.852	0.433	test
Rad_LR	0.815	0.731	0.713	0.8	train
	0.778	0.759	0.791	0.633	test
Rad_SVM	0.893	0.903	0.913	0.867	train
	0.686	0.683	0.696	0.633	test

In the test set, it had an AUC of 0.778, an accuracy of 0.759, a specificity of 0.791, and a sensitivity of 0.633. The Radiomics SVM model performed relatively well in the training set with an AUC of 0.893, an accuracy of 0.903, a specificity of 0.913, and a sensitivity of 0.867, but showed significant performance degradation in the test set with an AUC of 0.686, an accuracy of 0.683, a specificity of 0.696, and a sensitivity of 0.633. The DenseNet-264 deep learning model demonstrated superior performance with an AUC of 0.990 on the training set and 0.971 on the validation set. The radiomics model achieved an AUC of 0.815 on the training set and 0.778 on the validation set. These results indicate that the deep learning model outperforms the radiomics model in predicting bone metastasis in lung cancer patients. The high AUC values achieved by the DenseNet-264 model suggest that it can reliably identify patients at high risk of developing bone metastasis. This early prediction capability is crucial for timely intervention and personalized treatment planning. By accurately predicting bone metastasis, clinicians can implement more rigorous monitoring and tailored therapeutic strategies, potentially improving patient outcomes and quality of life.

3.3. Model comparison

- Comparison with traditional methods and other machine learning models

The performance of DenseNet-264 was rigorously compared to other models using the DeLong test, which assesses the statistical significance of differences in the AUCs of correlated ROC curves. The results, summarized in Table 4, indicate that DenseNet-264 significantly outperforms traditional radiomics models (Rad_KNN, Rad_LR, and Rad_SVM) and another deep learning model (DenseNet-121) across both the training and test sets.

For the training set, DenseNet-264's AUC was compared to that of DenseNet-121, Rad_KNN, Rad_LR, and Rad_SVM. The p-values for these comparisons were 0.08, 0.03, 0.02, and 0.04, respectively, showing that DenseNet-264 performs significantly better than Rad_KNN, Rad_LR, and Rad_SVM, with p-values less than 0.05. Although the p-value for the comparison with DenseNet-121 is slightly above 0.05, it still indicates a trend towards better performance.

In the test set, the p-values for comparing DenseNet-264 with DenseNet-121, Rad_KNN, Rad_LR, and Rad_SVM were similarly 0.08, 0.03, 0.02, and 0.04. This consistency across both training and test sets reinforces the robustness and generalizability of DenseNet-264. The significant p-values (<0.05) in comparisons with Rad_KNN, Rad_LR, and Rad_SVM indicate that DenseNet-264 has superior predictive accuracy in identifying bone metastasis in lung cancer patients.

The exceptional performance of DenseNet-264, particularly its higher AUC and robust generalizability, makes it a reliable and effective model for predicting bone metastasis. Its ability to significantly outperform traditional radiomics methods and other machine learning models underscores its potential for clinical application, providing a powerful tool for early detection and personalized treatment planning in lung cancer care. The Decision Curve Analysis (DCA) results are presented in Fig. 7. The DenseNet-264 model demonstrated higher net benefits across a range of threshold probabilities compared to the radiomics model and baseline models. This indicates that the DenseNet-264 model provides greater clinical utility by correctly identifying patients at risk of bone metastasis while minimizing unnecessary interventions. The net benefit curves suggest that using the DenseNet-264 model in clinical practice could improve decision-making and patient outcomes.

4. Discussion

This study presents significant advancements in predicting bone metastasis in lung cancer patients through the integration of radiomics and deep learning models. Our primary findings demonstrate that the DenseNet-264 deep learning model exhibits outstanding performance, achieving an AUC of 0.990 on the training set and 0.971 on the test set, which indicates excellent discriminative ability and generalizability. DenseNet-264 outperformed traditional radiomics models such as Rad_KNN, Rad_LR, and Rad_SVM, as well as another deep learning model, DenseNet-121, with higher accuracy, specificity, and sensitivity metrics. The p-values from the DeLong test further confirm the superior performance of DenseNet-264, with significant differences observed in comparisons with Rad_KNN, Rad_LR, and Rad_SVM (p-values < 0.05). Previous studies have explored the use of radiomics and traditional machine learning methods for predicting bone metastasis, with varying degrees of success. For instance, radiomics-based models have shown promise in capturing subtle imaging features associated with metastatic spread, but they often fall short in generalizability when applied to new dataset [4,29,30]. Our findings align with the literature in that radiomics features are valuable for prediction; however, the integration of deep learning, specifically the DenseNet-264 model, significantly enhances predictive performance. The DenseNet-264 model outperforms the radiomics model due to its ability to automatically learn complex features directly from raw CT images, leveraging deep learning techniques that capture intricate spatial patterns and hierarchical information. In contrast, the radiomics model relies on manually engineered features and lacks the depth and connectivity provided by the deep neural network, leading to suboptimal performance. The DenseNet-264 model outperforms the DenseNet-121 model due to its greater depth and dense connectivity, which enable it to capture more complex and abstract features, enhance feature reuse, and improve gradient flow. These architectural advantages lead to higher accuracy and robustness in

Table 4
DeLong test results comparing DenseNet-264 with other models.

Metric	Densnet-264 vs Densnet-121 (Train)	Densnet-264 vs Rad_KNN (Train)	Densnet-264 vs Rad_LR (Train)	Densnet-264 vs Rad_SVM (Train)	Densnet-264 vs Densnet-121 (Test)	Densnet-264 vs Rad_KNN (Test)	Densnet-264 vs Rad_LR (Test)	Densnet-264 vs Rad_SVM (Test)
p-value	0.08	0.03	0.02	0.04	0.08	0.03	0.02	0.04

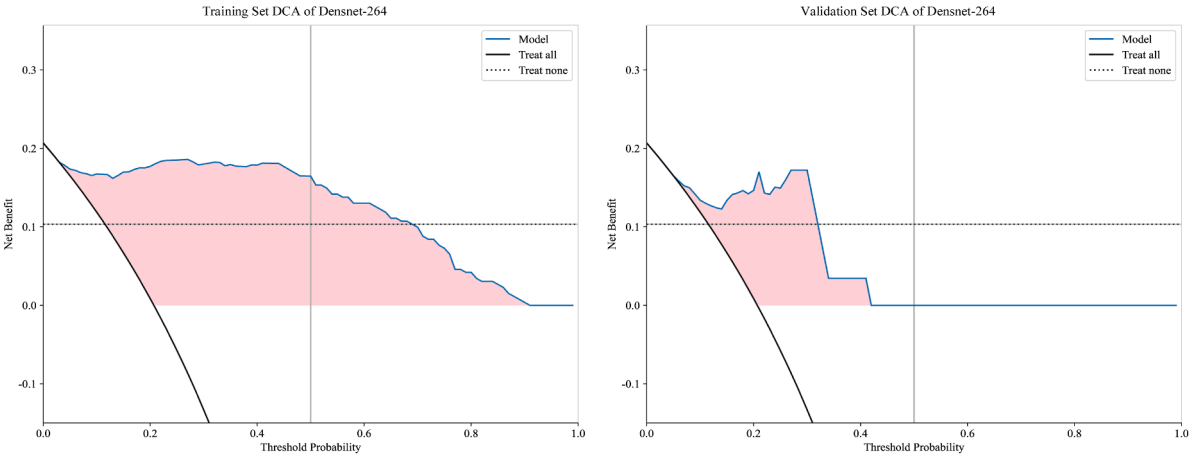

Fig. 7. Decision Curve Analysis (DCA) of the DenseNet-264 Model. The Decision Curve Analysis (DCA) plots for the DenseNet-264 model on the training set (left) and validation set (right). The y-axis represents the net benefit, while the x-axis represents the threshold probability. The solid blue line indicates the net benefit of the DenseNet-264 model, the black line represents the net benefit of the strategy of treating all patients as positive, and the dashed line represents the net benefit of treating no patients. The area under the blue line (shaded in pink) indicates the range of threshold probabilities where the model provides a net benefit over the "treat all" and "treat none" strategies. The DenseNet-264 model demonstrates higher net benefits across a range of threshold probabilities, indicating its clinical utility in predicting bone metastasis in lung cancer patients. (For interpretation of the references to colour in this figure legend, the reader is referred to the web version of this article.)

predicting bone metastasis. The results indicate that deep learning models can capture complex patterns and spatial dependencies in 3D CT images more effectively than traditional methods [31]. This study underscores the potential of advanced deep learning models, such as DenseNet-264, in improving the prediction of bone metastasis in lung cancer patients. By leveraging the strengths of radiomics and deep learning, our approach offers a robust and clinically applicable tool that outperforms existing methods, paving the way for more accurate and personalized patient care.

The findings of this study have important clinical implications for the prediction and management of bone metastasis in lung cancer patients. The superior performance of the DenseNet-264 deep learning model, with its high AUC, accuracy, specificity, and sensitivity, underscores its potential as a reliable tool for early prediction of bone metastasis. Early identification of patients at high risk for bone metastasis can lead to timely and more targeted therapeutic interventions, which may improve patient outcomes and quality of life [32]. For instance, patients identified as high-risk could be monitored more closely and provided with prophylactic treatments such as bisphosphonates or denosumab, which have been shown to delay the onset of skeletal-related events. Furthermore, the integration of such predictive models into clinical workflows can enhance decision-making processes, allowing oncologists to personalize treatment plans based on individual risk profiles [33]. This personalized approach could lead to more effective allocation of healthcare resources, reducing unnecessary treatments for low-risk patients and focusing intensive interventions on those who are most likely to benefit. Additionally, the use of advanced imaging and predictive analytics aligns with the broader trend toward precision medicine, where treatments are tailored to the specific characteristics of each patient's disease. Overall, the deployment of the DenseNet-264 model in clinical practice holds promise for improving the management of lung cancer patients, potentially leading to better prognosis and reduced morbidity associated with bone metastasis.[34] The integration of the DenseNet-264 model into clinical decision-making processes offers several advantages. By providing early predictions of bone metastasis, the model enables clinicians to identify high-risk patients sooner, allowing for prompt interventions. This can lead to improved patient outcomes through earlier initiation of treatment and closer monitoring. Furthermore, the model supports the development of personalized treatment plans by assessing individual risk levels, which can result in more targeted and effective therapies. The efficient identification of patients at higher risk also facilitates better resource allocation within healthcare systems, ensuring that intensive monitoring and treatment efforts are focused on those who need them most. Overall, the adoption of this predictive model has the potential to streamline clinical workflows, enhance patient care, and optimize resource utilization.

This study, while promising, has several limitations. The sample size of 189 patients may not capture the full variability of a larger, more diverse population [36]. Future research should include larger, multi-center datasets to enhance generalizability [37]. Additionally, the study relied solely on CT imaging; integrating other imaging modalities such as MRI and PET could provide a more comprehensive assessment and improve prediction accuracy. Such strategies are often implemented bycomputational techniquesfor prediction [38,39]. Moreover, the focus was exclusively on predicting bone metastasis without considering other metastatic sites. Future research should focus on validating these findings in larger, multi-center cohorts to ensure the robustness and generalizability of the predictive models across diverse populations and clinical settings. Combining imaging features with clinical and genomic data may further enhance the predictive accuracy and provide a more comprehensive risk assessment. Employing advanced automated segmentation techniques [40] can improve consistency and reduce potential biases introduced by manual segmentation [35,41].

5. Conclusion

This study demonstrates the potential of integrating radiomics and deep learning techniques to predict bone metastasis in lung cancer patients using chest CT images. The DenseNet-264 model exhibited superior performance compared to traditional radiomics models and other deep learning architectures, with high AUC, accuracy, specificity, and sensitivity across both training and test sets. These findings highlight the model's robust discriminative ability and generalizability, underscoring its potential for clinical application. The early and accurate prediction of bone metastasis can facilitate timely and targeted therapeutic interventions, improve patient outcomes, and optimize healthcare resource allocation.

CRediT authorship contribution statement

Taisheng Zeng: Writing – original draft, Project administration, Methodology, Formal analysis. **Yusi Chen:** Investigation. **Daxin Zhu:** Project administration, Methodology. **Yifeng Huang:** Investigation, Data curation. **Ying Huang:** Investigation, Data curation. **Yijie Chen:** Investigation, Data curation. **Jianshe Shi:** Investigation. **Bijiao Ding:** Data curation. **Jianlong Huang:** Project administration, Methodology.

Declaration of competing interest

This research is supported by the Fujian Provincial Natural Science Foundation of China (2023J01895) and the Science and Technology Program of Quanzhou (2021CT0010).

References

[1] H. Sung, et al., Global cancer statistics 2020: GLOBOCAN estimates of incidence and mortality worldwide for 36 cancers in 185 countries, CA Cancer J. Clin. 71 (2021) 209–249, https://doi.org/10.3322/caac.21660.
[2] R.S. Herbst, D. Morgensztern, C. Boshoff, The biology and management of non-small cell lung cancer, Nature 553 (2018) 446–454, https://doi.org/10.1038/nature25183.
[3] C. D'Antonio, et al., Bone and brain metastasis in lung cancer: recent advances in therapeutic strategies, Ther. Adv. Med. Oncol. 6 (2014) 101–114, https://doi.org/10.1177/1758834014521110.
[4] R.E. Coleman, Clinical features of metastatic bone disease and risk of skeletal morbidity, Clin. Cancer Res. 12 (2006) 6243s–s6249, https://doi.org/10.1158/1078-0432.Ccr-06-0931.
[5] M. Kuchuk, C.L. Addison, M. Clemons, I. Kuchuk, P. Wheatley-Price, Incidence and consequences of bone metastases in lung cancer patients, J. Bone Oncol. 2 (2013) 22–29, https://doi.org/10.1016/j.jbo.2012.12.004.
[6] S. Vicent, N. Perurena, R. Govindan, F. Lecanda, Bone metastases in lung cancer. Potential novel approaches to therapy, Am. J. Respir. Crit. Care Med. 192 (2015) 799–809, https://doi.org/10.1164/rccm.201503-0440SO.
[7] B.J. Knapp, S. Devarakonda, R. Govindan, Bone metastases in non-small cell lung cancer: a narrative review, J. Thorac. Dis. 14 (2022) 1696–1712, https://doi.org/10.21037/jtd-21-1502.
[8] S. Ricciardi, F. de Marinis, Treatment of bone metastases in lung cancer: the actual role of zoledronic acid, Rev. Recent Clin. Trials 4 (2009) 205–211, https://doi.org/10.2174/157488709789957718.
[9] R. Coleman, et al., Consensus on the utility of bone markers in the malignant bone disease setting, Crit. Rev. Oncol. Hematol. 80 (2011) 411–432, https://doi.org/10.1016/j.critrevonc.2011.02.005.
[10] H. Katagiri, et al., Prognostic factors and a scoring system for patients with skeletal metastasis, J. Bone Joint Surg. Br. 87 (2005) 698–703, https://doi.org/10.1302/0301-620x.87b5.15185.
[11] S.L. Wood, J.A. Westbrook, J.E. Brown, Omic-profiling in breast cancer metastasis to bone: implications for mechanisms, biomarkers and treatment, Cancer Treat. Rev. 40 (2014) 139–152, https://doi.org/10.1016/j.ctrv.2013.07.006.
[12] K.N. Weilbaecher, T.A. Guise, L.K. McCauley, Cancer to bone: a fatal attraction, Nat. Rev. Cancer 11 (2011) 411–425, https://doi.org/10.1038/nrc3055.
[13] J. Chudacek, et al., Detection of minimal residual disease in lung cancer, Biomed. Pap. Med. Fac. Univ. Palacky Olomouc Czech Repub. 158 (2014) 189–193, https://doi.org/10.5507/bp.2013.019.
[14] J. Pretell-Mazzini, C.S. Seldon, G. D'Amato, T.K. Subhawong, Musculoskeletal metastasis from soft-tissue sarcomas: a review of the literature, J. Am. Acad. Orthop. Surg. 30 (2022) 493–503, https://doi.org/10.5435/jaaos-d-21-00944.
[15] L.S. Ter Maat, et al., CT radiomics compared to a clinical model for predicting checkpoint inhibitor treatment outcomes in patients with advanced melanoma, Eur. J. Cancer 185 (2023) 167–177, https://doi.org/10.1016/j.ejca.2023.02.017.
[16] R.J. Cook, P. Major, Multistate analysis of skeletal events in patients with bone metastases, Clin. Cancer Res. 12 (2006) 6264s–s6269, https://doi.org/10.1158/1078-0432.Ccr-06-0654.
[17] E. Faiella, et al., Artificial intelligence in bone metastases: an MRI and CT imaging review, Int. J. Environ. Res. Public Health 19 (2022), https://doi.org/10.3390/ijerph19031880.
[18] J.W. Fletcher, et al., Recommendations on the use of 18F-FDG PET in oncology, J. Nucl. Med. 49 (2008) 480–508, https://doi.org/10.2967/jnumed.107.047787.
[19] P. Lambin, et al., Radiomics: extracting more information from medical images using advanced feature analysis, Eur. J. Cancer 48 (2012) 441–446, https://doi.org/10.1016/j.ejca.2011.11.036.
[20] R.J. Gillies, P.E. Kinahan, H. Hricak, Radiomics: images are more than pictures, They are data, Radiology 278 (2016) 563–577, https://doi.org/10.1148/radiol.2015151169.
[21] A. Esteva, et al., Dermatologist-level classification of skin cancer with deep neural networks, Nature 542 (2017) 115–118, https://doi.org/10.1038/nature21056.
[22] H.J. Aerts, et al., Decoding tumour phenotype by noninvasive imaging using a quantitative radiomics approach, Nat. Commun. 5 (2014) 4006, https://doi.org/10.1038/ncomms5006.
[23] K.G. van Leeuwen, S. Schalekamp, M. Rutten, B. van Ginneken, M. de Rooij, Artificial intelligence in radiology: 100 commercially available products and their scientific evidence, Eur. Radiol. 31 (2021) 3797–3804, https://doi.org/10.1007/s00330-021-07892-z.
[24] W.L. Bi, et al., Artificial intelligence in cancer imaging: clinical challenges and applications, CA Cancer J. Clin. 69 (2019) 127–157, https://doi.org/10.3322/caac.21552.
[25] H. Peng, F. Long, C. Ding, Feature selection based on mutual information: criteria of max-dependency, max-relevance, and min-redundancy, IEEE Trans. Pattern Anal. Mach. Intell. 27 (2005) 1226–1238, https://doi.org/10.1109/tpami.2005.159.
[26] Y. Li, F. Lu, Y. Yin, Applying logistic LASSO regression for the diagnosis of atypical Crohn's disease, Sci. Rep. 12 (2022) 11340, https://doi.org/10.1038/s41598-022-15609-5.
[27] F. Hong, L. Tian, V. Devanarayan, Improving the robustness of variable selection and predictive performance of regularized generalized linear models and cox proportional hazard models, Mathematics (Basel) 11 (2023), https://doi.org/10.3390/math11030557.
[28] A.J. Vickers, Decision analysis for the evaluation of diagnostic tests, prediction models and molecular markers, Am. Stat. 62 (2008) 314–320, https://doi.org/10.1198/000313008x370302.
[29] L. Jin, et al., Breast cancer lung metastasis: molecular biology and therapeutic implications, Cancer Biol. Ther. 19 (2018) 858–868, https://doi.org/10.1080/15384047.2018.1456599.
[30] C.A. Valette, et al., Treatment patterns and clinical outcomes of extensive stage small cell lung cancer (SCLC) in the real-world evidence ESME cohort before the era of immunotherapy, Respir. Med. Res. 84 (2023) 101012, https://doi.org/10.1016/j.resmer.2023.101012.
[31] G. Huang, Z. Liu, K.Q. Weinberger. Densely Connected Convolutional Networks. *2017 IEEE Conference on Computer Vision and Pattern Recognition (CVPR)*, 2261-2269 (2016).
[32] T.H. Witney, D.Y. Lewis, Imaging cancer metabolism with positron emission tomography (PET), Methods Mol. Biol. 1928 (2019) 29–44, https://doi.org/10.1007/978-1-4939-9027-6_2.
[33] D.H. Henry, et al., Randomized, double-blind study of denosumab versus zoledronic acid in the treatment of bone metastases in patients with advanced cancer (excluding breast and prostate cancer) or multiple myeloma, J. Clin. Oncol. 29 (2011) 1125–1132, https://doi.org/10.1200/jco.2010.31.3304.
[34] K. Sies, et al., Dark corner artefact and diagnostic performance of a market-approved neural network for skin cancer classification, J. Dtsch. Dermatol. Ges. 19 (2021) 842–850, https://doi.org/10.1111/ddg.14384.
[35] J.J.M. van Griethuysen, et al., Computational radiomics system to decode the radiographic phenotype, Cancer Res. 77 (2017) e104–e107, https://doi.org/10.1158/0008-5472.Can-17-0339.
[36] Y. Shao, Y. Yin, Du. Shichang, T. Xia, L. Xi, Leakage monitoring in static sealing interface based on three dimensional surface topography indicator, ASME Trans. Manuf. Sci. Eng. 140 (10) (2018) 101003.
[37] D. Huang, Du. Shichang, G. Li, Wu. Zhuoqi, A systematic approach for on-line minimizing volume difference of multiple chambers in machining processes based on high definition metrology, ASME Trans. Manuf. Sci. Eng. 139 (8) (2017).
[38] Du. Shichang, L. Fei, Co-Kriging method for form error estimation incorporating condition variable measurements, ASME Trans. J. Manuf. Sci. Eng. 138 (2016).
[39] G. Li, Du. Shichang, Elastic mechanics-based fixturing scheme optimization of variable stiffness structure workpieces for surface quality improvement, Precis. Eng. 56 (2019) 343–363.
[40] C. Zhao, J. Lv, D. Shichang, Geometrical deviation modeling and monitoring of 3D surface based on multi-output gaussian process, Measurement 199 (2022) 111569.
[41] K.K.L. Wong. Cybernetical Intelligence: Engineering Cybernetics with Machine Intelligence, *John Wiley & Sons*, Inc., Hoboken, New Jersey, ISBN: 9781394217489, 2023.